PCCP

PAPER

View Article Online
View Journal

Cite this: DOI: 10.1039/c8cp01619d

Time-resolved spectroscopy of the ensembled photoluminescence of nitrogen- and boron/nitrogen-doped carbon dots†

Sunghu Kim,‡[a] Byung-Kuk Yoo,‡[b] Yuri Choi,[a] Byeong-Su Kim[ac] and Oh-Hoon Kwon*[a]

Received 13th March 2018,
Accepted 11th April 2018

DOI: 10.1039/c8cp01619d

rsc.li/pccp

Carbon dots (CDs) have potential applications in various fields such as energy, catalysis, and bioimaging due to their strong and tuneable photoluminescence (PL), low toxicity, and robust chemical inertness. Although several PL mechanisms have been proposed, the origin of PL in CDs is still in debate because of the ensembled nature of the heterogeneous luminophores present in the CDs. To unravel the origin of PL in CDs, we performed time-resolved spectroscopy on two types of CDs: nitrogen-doped (N-CD) and boron–nitrogen co-doped (BN-CD). The PL decays were fitted by stretched exponential functions to estimate the distribution of the decay kinetics in the CDs, which have different PL lifetime distributions. Both CDs displayed main, blue emission decaying in 15 ns, which originates from the dominant molecular state. The analysis of the non-exponential PL decay using stretched exponential fits revealed that the functional surface luminophores are of less variety but of more environmental heterogeneity and have much lower populations in BN-CD than in N-CD.

1. Introduction

Carbon dots (CDs) have recently been highlighted as promising nanomaterials for optoelectronics, bioimaging, photocatalysts, biosensors, drug delivery, and solar light harvesting.[1–7] CDs are considered a new class of fluorescent nanoparticles of quasi-spherical shape and sub-10 nm size. They possess many advantages such as wide-range photoluminescence (PL), low toxicity, biocompatibility, and photostability.[2] CDs generally consist of a few-layer graphitic structure and various organic functional groups on the surface. Various synthetic routes have been developed using bottom-up and top-down approaches to enhance the PL performance of CDs. The top-down method is based on the exfoliation or oxidation of precursors through electrochemical oxidation, laser ablation, and arc charge from bulk carbon materials.[8–10] The bottom-up process is a synthetic route to build CDs from small molecules using various organic precursors. In particular, hydrothermal, pyrolysis, and microwave-assisted methods are widely used owing to their synthetic feasibility.[11–13]

The PL quantum yield (QY) is a key parameter for preparing highly fluorescent materials. However, CDs have typically low quantum yields unless they are chemically modified.[14] Thus, numerous approaches have been developed to enhance the PL QY of CDs: doping with heterogeneous atoms, reduction on the surface, surface passivation, adopting different synthetic conditions, and using different precursors.[15–18] Unlike conventional fluorescent dyes, CDs have unique PL properties including excitation-wavelength (λ_{ex})-dependence, which leads to low PL QY.[19] Therefore, active research efforts have been directed towards adopting surface passivation,[20] different synthetic methods,[21] and various synthetic conditions such as pH and solvents to reduce the λ_{ex}-dependence and enhance the PL QY.[22–24] Most recently, the highest PL QY (up to 94%) of graphene quantum dots was obtained through a hydrothermal method using various nitrogen (N) precursors.[18] Although the origin of PL in carbon-based nanomaterials including CDs is still an open debate,[25,26] several mechanisms based on quantum confinement effects and conjugated π-domains,[3,27] the role of surface functional groups with different electronic transitions,[28,29] and the formation of fluorescent molecules on the surface or inside the CDs (molecular state) have been proposed.[30,31] Bhattacharya *et al.* observed a wide size distribution

[a] Department of Chemistry, School of Natural Science, Ulsan National Institute of Science and Technology (UNIST), Ulsan 44919, Korea. E-mail: ohkwon@unist.ac.kr
[b] Division of Chemistry and Chemical Engineering, California Institute of Technology, Pasadena, CA 91125, USA
[c] Department of Energy Engineering, School of Energy and Chemical Engineering, Ulsan National Institute of Science and Technology (UNIST), Ulsan 44919, Korea

† Electronic supplementary information (ESI) available: Normalized PL spectra; deconvoluted PL spectra; TRANES; time-resolved PL of BN-CD by excitation at 450 nm; TRES of N-CD by different fitting. See DOI: 10.1039/c8cp01619d

‡ Equally contributed to this work.

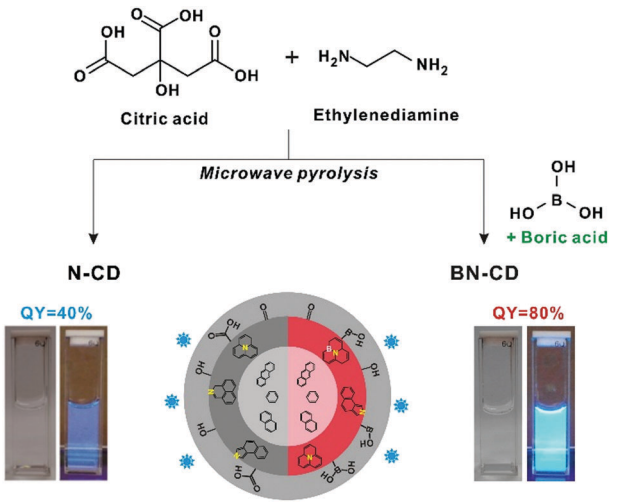

Scheme 1 Synthetic scheme and chemical structure of N-CD and BN-CD.

in CDs with atomic force microscopy and concluded that the λ_{ex}-dependence of the PL originates from the quantum confinement effect rather than the distribution of different surface trap states.[27] Bao *et al.* prepared CDs with different degrees of surface oxidation by an electrochemical method and attributed the PL to the specific molecular configurations of oxygen-based surface groups.[32] Song *et al.* synthesized CDs by a hydrothermal route using citric acid and ethylenediamine (EDA) as precursors. Interestingly, they isolated a fluorescent citrazinic acid derivative, imidazo[1,2*a*]pyridine-7-carboxylic acid (IPCA), from the CDs and proposed that IPCA is responsible for the strong blue emission, *i.e.* molecular-state PL.[31] Our group has recently reported significant enhancement in the PL QY of boron (B)- and (N)-co-doped CD (BN-CD) compared to that of N-doped CD (N-CD) due to the suppressed development of heterogeneous surface states, characterized by various spectroscopic measurements coupled with density functional theory calculations (Scheme 1).[14] The additional B-doping resulted in different configurations of C and N atoms and surface functional groups. For instance, the major N and O groups in N-CD were pyrrolic nitrogen and carboxylic groups, whereas graphitic N and carbonyl and hydroxyl groups were present in BN-CD. The reduction of non-radiative recombination from deep trap states was proposed to originate from the formation of fewer surface states and more graphitic structures in BN-CD, resulting in improved optical properties of BN-CD not only in aqueous (QY = 80%) but also in the solid (QY = 67%) state.

Herein, we systematically investigate both the static and time-resolved optical properties of the two doped CDs (N-CD and BN-CD) to clarify the origin of the improved PL of BN-CD. The presence of various emissive states in these CDs results in complicated time-dependent behaviour of the PL. Therefore, to quantify the ensemble character of these multiple emissive states, the PL decay profiles of each CD across the entire visible range were uniquely analysed by using stretched-exponential functions. This approach clearly contrasts with our previous contribution which focused on the synthesis of both N-CD and BN-CD and analysis of their photophysical properties by using arbitrary multi-exponential functions.[14] The comparison of the PL lifetime distributions of the two CDs confirmed that the blue PL mainly originates from the molecular state. The influence of the various surface chromophores on the PL and the quantitative characterization of ensemble emissive states are discussed.

2. Experimental

2.1. Materials

The detailed procedure for the synthesis of N-CD and BN-CD has been reported elsewhere.[14] Briefly, BN-CD was prepared through microwave pyrolysis of citric acid, EDA, and boric acid. As a control, N-CD was synthesized with identical precursors except for boric acid.

2.2. Measurements

Absorption spectra were obtained by using a UV-vis spectrometer (V-730, Jasco) and steady-state fluorescence spectra were obtained by using a fluorometer (RF-6000, Shimadzu). PL lifetimes were measured with a time-correlated single photon counting spectrometer (FluoTime 300, PicoQuant) with a light source of picosecond-pulsed diode lasers emitting at 375 nm (LDH-D-C-375, PicoQuant) and at 450 nm (LDH-D-C-450, PicoQuant). The total instrument response function (IRF) was approximately 190 ps. All fluorescence decay profiles were fitted to stretched-exponential functions by using the FluoFit software (PicoQuant).

3. Results and discussion

3.1. Steady-state absorption spectra

The absorption spectra of both CDs in the UV-visible region are shown in Fig. 1. Each absorption spectrum exhibits a weak shoulder at 250 nm and a prominent peak at 350 nm. According to previous reports,[14,31] these spectral features are ascribed to the superposition of the absorption by a molecular state of IPCA and the sp^2-carbon core and surface functional groups of the CD chromophores. Specifically, IPCA has been reported to show strong absorption bands at 240 nm and 350 nm.[31] Typically, CDs show absorption bands at ~230, ~280, and ~320 nm, the first being attributed to the π–π* transition of the sp^2-carbon core (C=C) and the other two to the n–π* transitions of carbonyl-bearing (C=O) functional groups.[19] As the band structures at ~280 and ~320 nm are not discernible, the overall absorption features for both CDs are inferred to originate mainly from the molecular state. In addition, N-CD has an extra absorption in the visible region beyond 410 nm, indicating the presence of lower energy states from N-related functional groups, *i.e.*, N-related defects,[33] in contrast to BN-CD. Wang *et al.* also suggested that the N defects contribute to the absorption tail in the visible range around ~450 nm.[34] N-CDs have been shown to exclusively possess pyrrolic N groups.[14] In the BN-CDs, the introduction of the less electronegative B atoms accommodates the charge density of the C and N bonding matrix, causing a change in the bonding

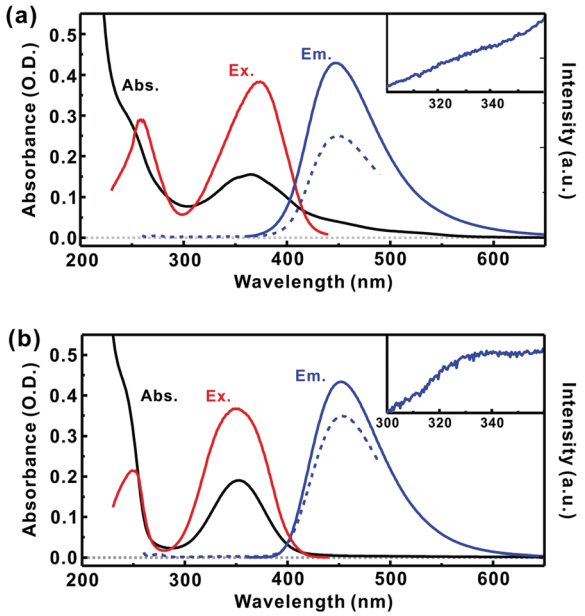

Fig. 1 Optical spectra of N-CD and BN-CD in aqueous solution: absorption (black solid); excitation (red solid); and emission (blue solid and dashed) for (a) N-CD and (b) BN-CD. The emission spectra were measured by excitation at 250 nm (blue dashed) and 350 nm (blue solid). The excitation spectra were measured by emission at 450 nm. Each inset shows the magnified emission spectrum with excitation at 250 nm.

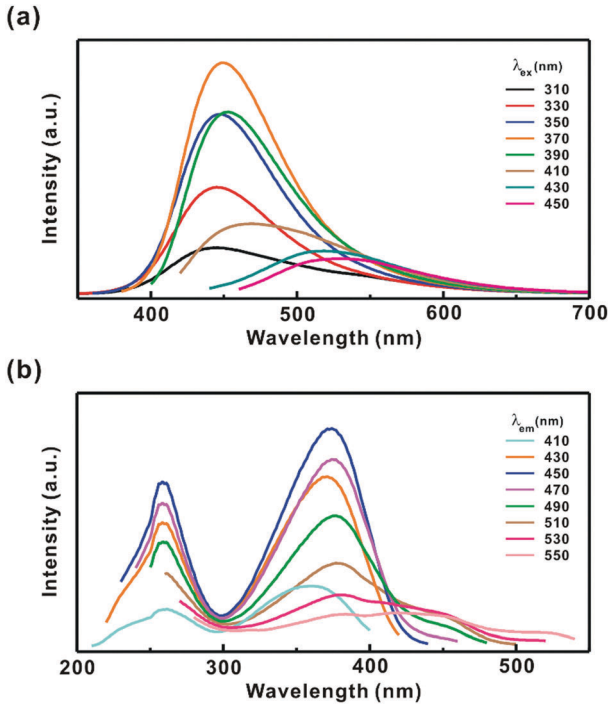

Fig. 2 (a) PL spectra with varying excitation wavelengths from 310 to 450 nm and (b) excitation spectra with varying emission wavelengths from 410 to 550 nm with 20 nm increments for N-CD.

patterns, which subsequently increases the amount of graphitic C and N in the matrix and decreases the number of surface states. Consequently, the additional doping of B suppresses the formation of N-related functional groups on the surface of the BN-CD.

3.2. Steady-state PL spectra

As seen in Fig. 1, the PL peaks of both CDs are located at ~450 nm with excitation at 350 nm. The PL excitation spectra show two peaks at ~250 nm and ~350 nm when monitored at 450 nm. The insets show the magnified PL spectra; a hint of a shoulder structure at ~330 nm is observed when excited at 250 nm and the band feature is more pronounced for BN-CD. The origin of the weak PL band at 330 nm is assigned to the π–π* transition of the C core. The much weaker PL peak at ~330 nm compared to that at ~450 nm may be a feature of the energy transfer from the carbon core to the molecular state and/or the surface states. The wavelength of the PL (330 nm) excited at 250 nm matches with the one of the two strong bands (at ~250 nm and ~350 nm) in the PL excitation spectra that satisfies the condition for efficient energy transfer.

As shown in Fig. 2a and Fig. S1a (ESI†), the PL spectra of N-CD exhibited strong λ_{ex}-dependent behaviour owing to the multiple emissive states on the surface. In the PL excitation spectra of N-CD (Fig. 2b and Fig. S1b, ESI†), the peaks are located at ~260 nm, ~350–380 nm, ~420 nm, ~450 nm, and ~520 nm, the sum of which appears as the broad tail beyond 410 nm in the absorption spectrum in Fig. 1a. In comparison, the maximum of the PL peak of the BN-CD is centred at ~450 nm regardless of λ_{ex} (Fig. 3a). When normalized, the PL spectra show an additional band centred at ~520 nm (Fig. S2a, ESI†). In addition, the PL excitation spectra of BN-CD show mainly two peaks at ~250 nm and ~350 nm (Fig. 3b and Fig. S2b, ESI†). The bands at ~450 nm and ~530 nm observed in N-CD were greatly suppressed in BN-CD. Based on these results, we attribute the bands in the visible range of the PL excitation spectra to multiple emissive surface states responsible for the λ_{ex}-dependent PL behaviour. As previously reported, the emission of carbon-based nanomaterials generally depends on λ_{ex}.[21,35–37] In addition, surface oxidation or reduction plays a crucial role in forming multiple emissive electronic states in some CDs.[33] Nevertheless, a much weaker dependence on λ_{ex} was found for the BN-CDs, which indicates that individual BN-CDs contain fewer multi-chromophoric units.

3.3. Time-resolved PL decay

Previous interpretation of the PL lifetimes of CDs using fits with multi-exponential functions were based on the measurements with time-correlated single photon counting (TCSPC) and fluorescence upconversion spectroscopy; tri-exponential functions were used to fit the PL profiles obtained from TCSPC spectroscopy on the timescale of a few hundred ps and longer.[14] In a previous study, decay profiles around the PL peaks (430–480 nm) with λ_{ex} of 375 nm were obtained; they show 15 ns and 500 ps components for both CDs and an additional 5 ns component exclusively for N-CD. Herein, we extended the probed region to cover longer wavelengths (up to 650 nm) and λ_{ex} in TCSPC spectroscopy measurements. Fig. 4 presents the time-resolved PL profiles of N-CDs (left) and BN-CDs (right) at

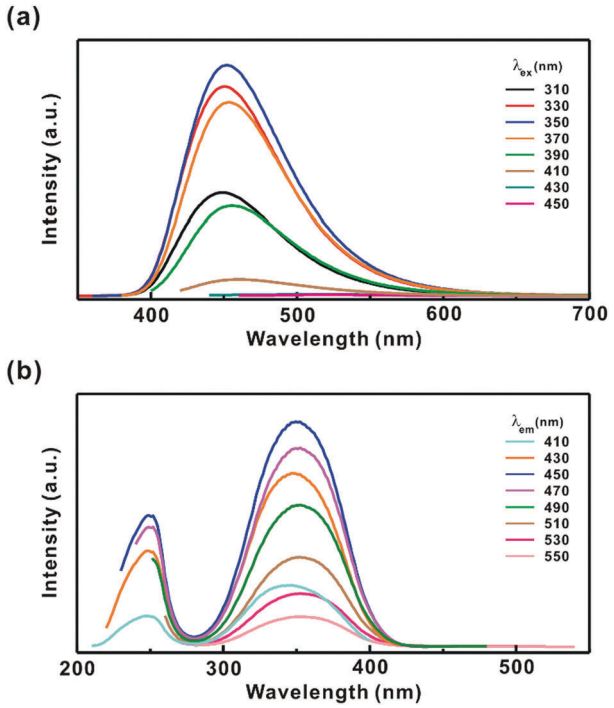

Fig. 3 (a) PL spectra with varying excitation wavelengths from 310 to 450 nm and (b) excitation spectra with varying emission wavelengths from 410 to 550 nm with 20 nm increments for BN-CD.

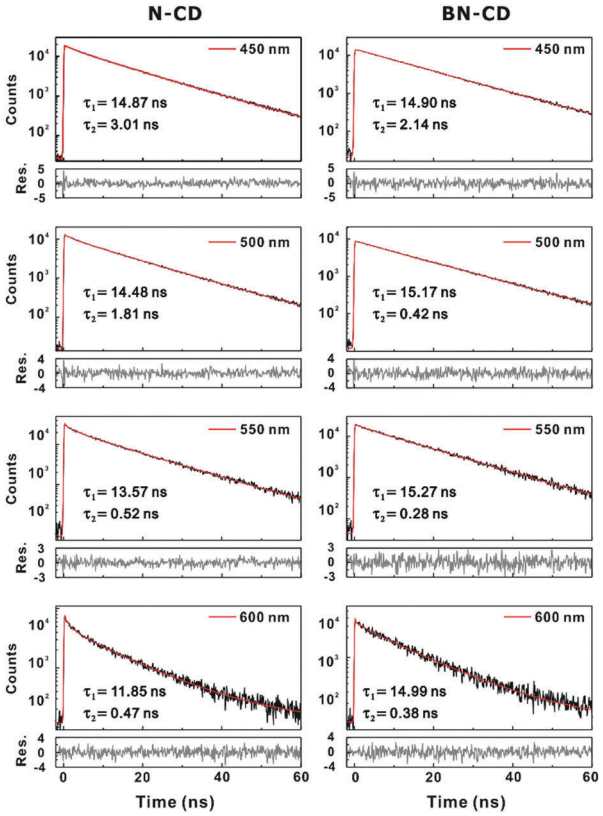

Fig. 4 Photoluminescence decay profiles of N-CD (left panels) and BN-CD (right panels) with excitation at 375 nm. Fits and monitored wavelengths are given in each panel. The residuals of the fits are also shown below each panel. Fit parameters are listed in Table 1.

several representative wavelengths. Overall, the decay times for N-CD become faster as the probe wavelength increases. This effect was not significant for BN-CD, as seen from the weaker dependence on the probe wavelength. If all decay profiles at given emission wavelengths are analysed with multi-exponential functions, the fit results do not necessarily possess a physical meaning because the same decay profile may also be adequately fitted by various combinations of the exponential components. Moreover, at least three exponential components were necessary to fit the PL decay profile of N-CD for each λ_{ex}. When a global analysis was applied, each lifetime component had different spectral features in terms of both peak position and bandwidth (Fig. S3, ESI†). One approach to mitigate the limitations in the fit of the non-exponential behaviour of PL decay, which originates from multiple emissive states, is the use of stretched-exponential functions with a minimal number of components. Such functions are commonly used to describe the luminescence decay dynamics of disordered systems of complex luminophores.[38] Therefore, for systems having multiple emissive states and which are not well-defined, stretched-exponential functions can be employed for the quantitative analysis of the distribution of the emissive states, representative lifetimes, and fractions of the constituent components.

To elucidate the origin of the different dynamic behaviours of the two CDs, all decay profiles were fitted using the stretched exponential function $I(t)$:

$$I(t) = \sum_{i}^{n} A_i \exp\left(-\frac{t}{\tau_i}\right)^{\beta_i},$$

where τ_i denotes the PL lifetimes; β_i is a distribution parameter; and A_i is the amplitude of each component. β indicates the distribution of the PL lifetimes, where a smaller β means a wider distribution. Because of the possible role of the molecular state and of an ensemble of emitting surface states in the PL decay, two stretched exponential components are considered ($n = 2$). Fit results for both CDs are summarized in Table 1. The fractional amplitudes of the τ_1 component at 450 nm are dominant in both CDs, with values of 0.76 and 0.93 in N-CD and BN-CD, respectively. As the emission probe wavelength increases, the fractional amplitudes of the τ_1 components decrease and those of the τ_2 components increase in both CDs, although the PL lifetimes τ_2 are similar in both cases.

The decrease in τ_1 and β_1 with the increase in emission wavelength is noticed only in N-CD, with a dominant decay time of $\tau_1 \sim 15$ ns, which is almost the same as previously reported for CDs complexed with the IPCA fluorophore.[31] On the other hand, the second decay time (τ_2) varies from ~100 ps to 3 ns (depending on the emission wavelength) for N-CD and from ~300 ps to 2 ns for BN-CD. For both CDs, the distribution factor β was mostly equal to 1 for the first component ($\tau_1 \sim 15$ ns) in a wide range of emission wavelengths, confirming the assignment of the 15 ns component to the molecular state. As seen in Table 1, β_2 varies with the emission wavelength for both CDs; the ranges of β_2 values are 0.3–0.8 and

Table 1 Fit parameters of the stretched-exponential function for both CDs with excitation at 375 nm and 450 nm

CD	λ_{ex}[a] (nm)	λ_{em}[b] (nm)	A_1	τ_1 (ns)	β_1[c]	A_2	τ_2 (ns)	β_2
N-CD	375	450	0.76 ± 0.01	14.87 ± 0.05	1.00	0.24 ± 0.01	3.01 ± 0.17	0.78 ± 0.04
		500	0.68 ± 0.01	14.48 ± 0.06	0.99	0.32 ± 0.02	1.81 ± 0.09	0.51 ± 0.01
		550	0.57 ± 0.02	13.57 ± 0.11	0.96 ± 0.01	0.43 ± 0.03	0.52 ± 0.08	0.45 ± 0.03
		600	0.50 ± 0.03	11.85 ± 0.25	0.90	0.50 ± 0.05	0.47 ± 0.13	0.55 ± 0.10
	450	500	0.59 ± 0.03	5.26 ± 0.02	0.78	0.41 ± 0.01	0.20 ± 0.01	0.52 ± 0.02
		550	0.63 ± 0.03	5.38 ± 0.02	0.80	0.37 ± 0.02	0.20 ± 0.02	0.57 ± 0.04
		600	0.46 ± 0.03	5.08 ± 0.03	0.82	0.54 ± 0.01	0.13 ± 0.01	0.34
BN-CD	375	450	0.93 ± 0.01	14.90 ± 0.05	1.00 ± 0.01	0.07	2.14 ± 0.13	0.35 ± 0.01
		500	0.83 ± 0.02	15.17 ± 0.06	1.00 ± 0.01	0.17 ± 0.02	0.42 ± 0.04	0.31 ± 0.01
		550	0.73 ± 0.05	15.27 ± 0.13	1.00 ± 0.01	0.27 ± 0.07	0.28 ± 0.10	0.36 ± 0.03
		600	0.62 ± 0.07	14.99 ± 0.43	1.00 ± 0.03	0.38 ± 0.11	0.38 ± 0.13	0.31 ± 0.02

[a] Excitation wavelength. [b] Monitored emission wavelength. [c] Distribution parameter of stretched exponential functions.

0.3–0.4 for N-CD and BN-CD, respectively. It follows that the distribution of τ_2 is widely spread for both CDs, with β values much lower than 1. The PL of CDs with λ_{ex} = 375 nm can be divided into two categories: the first component arises from the molecular state, and the second component from the heterogeneous surface states with much shorter τ values and smaller β values.[33,39,40] The molecular state is found to be the main source of the absorption around 350 nm because of the major fraction of the 15 ns component in the total PL decay.

A variety of surface states resulted in the λ_{ex}-dependence of the PL. Roding *et al.* reported that the fitting of the PL lifetimes of graphene quantum dots resulted in two distinct systems: a homogeneous, fluorescein dye system and a highly heterogeneous graphene quantum dot system.[41] The fraction of molecular states with long PL decay times responsible for the increased PL QY is larger than the fraction of short-lived surface states in BN-CD and N-CD. The short-lived surface states are less developed in BN-CD as seen in Table 1 (A_2); the lower β value in BN-CD than in N-CD infers that the surface states experience more heterogeneity in terms of environment and the size of π domains (see below).

3.4. Time-resolved PL spectra

To quantify the PL originating from the multiple emitting states of both CDs in terms of different lifetimes and spectral positions, time-resolved emission spectra (TRES)[20] were constructed from 400 to 650 nm with 5 nm increments. The TRES peaks are centred at ~450 nm with an excitation at 375 nm for both CDs (Fig. 5a and 6a). In the time-resolved area normalized emission spectra (TRANES) of N-CD, no spectral shift occurred, and isoemissive points are barely observed at 430 and 530 nm (Fig. S4, ESI†). Isoemissive points in TRANES generally indicate the existence of multiple emissive states, thus hinting that N-CD may have multiple emissive states when excited at 375 nm.[42] Isoemissive points were not discerned for BN-CD.

All time-resolved PL profiles in the 400–650 nm range were fitted by double stretched-exponential functions every 5 nm for both CDs. The fitting parameters for the PL lifetimes (τ_i), amplitudes (A_i), and distribution of lifetimes (β_i) of each profile are given for the probed range of wavelengths for both CDs in Fig. 5b–d and 6b–d. When β, τ, and A are plotted as a function of the emission wavelength, those plots can be interpreted as an advanced spectral mapping of each parameter. For example, if $0 < \beta < 1$, β represents the degree of individual rate variation in CDs (the smaller β, the larger the distribution), and significantly different τ values for various wavelengths may indicate the existence of emitting states of different origin. Therefore, the plots of the pre-exponential factors (amplitude) of such stretched-exponential functions as a function of wavelength reveal the spectral envelope and wavelength of the emissive states. As shown in Fig. 5b and 6b, the pre-exponential factors for the second component (A_2) with smaller τ are smaller for BN-CD, in accordance with the higher QY of BN-CD than of N-CD.[14] This result is in line with the previous structural study, which explained the enhanced QY of BN-CD from the suppression of the formation of N-related defects by the insertion of B atoms.[14]

For both CDs, the major pre-exponential amplitude A_1 reaches a maximum at 450 nm, which corresponds to τ_1 = ~15 ns and β_1 = 1, and originates from the molecular state previously observed in a homogeneous CD system containing the bright blue fluorophore IPCA.[31,43] As shown in Fig. 5c and 6c, N-CD shows a disordered distribution of PL lifetimes for the range of probed wavelengths with β_2 = ~0.6 and τ_2 spanning 500 ps to 3 ns, compared to BN-CD with β_2 = ~0.3 and τ_2 = ~500 ps. The smaller variation of τ_2 values over a wide range of wavelengths indicate the less heterogeneity in the entities of surface functional groups of BN-CD because of the co-doping, which induces a smaller fraction of N-related defects because the graphitic N configuration is more dominant. The smaller β values, however, may indicate that the size distribution of π-conjugated sp^2-domains related to the surface functional groups is wider for BN-CD or that such surface luminophores experience more heterogeneous local environments. The second lifetime τ_2 decreases as the probed wavelength increases, as shown in Fig. 5d and 6d. This effect can be understood in terms of the energy gap law, which predicts that the decay time generally decreases when the energy gap between the ground and excited states decreases. Also, the possible role of energy transfer among emitting states with slightly different energy levels cannot be ruled out. Noticeably, β_1 and τ_1 only decrease at longer wavelengths from ~550 nm for N-CD but are relatively constant in BN-CD throughout the probed range. With the 15 ns component assigned to the molecular state, the global fitting of

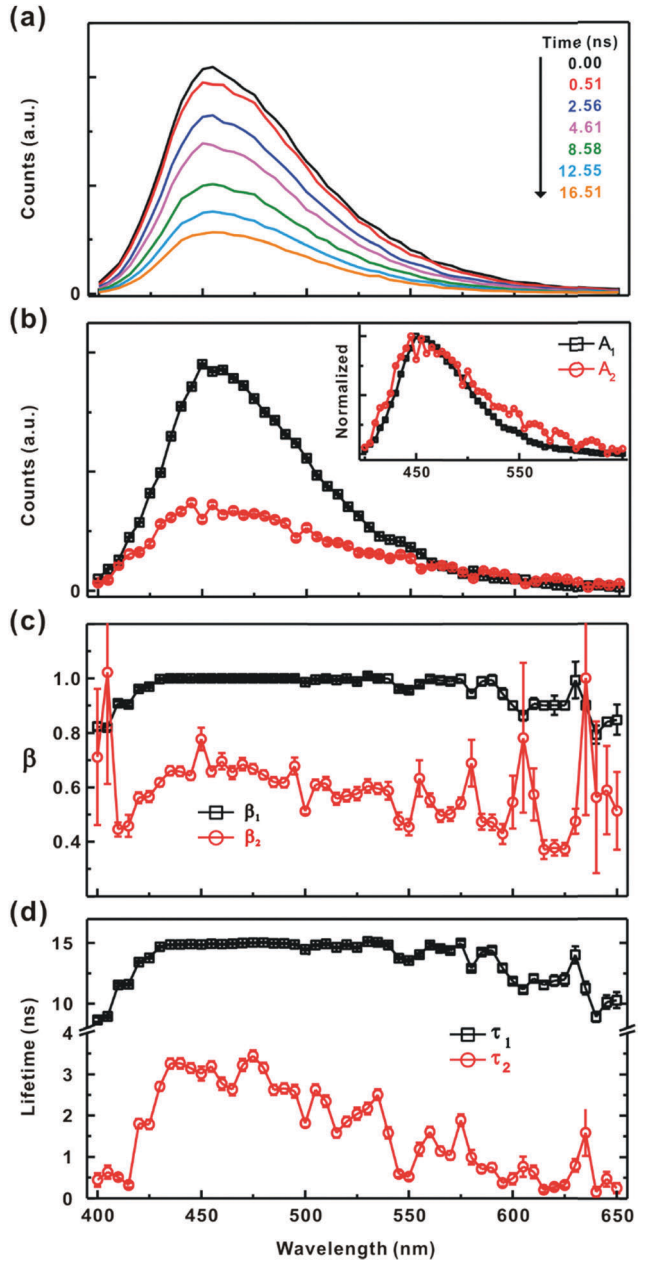

Fig. 5 (a) Time-resolved emission spectra (TRES) of N-CD with excitation wavelength at 375 nm. Fitting parameters from the stretched-exponential functions are as follows: (b) amplitudes (A_i) of the fluorescence lifetimes; (c) distribution factors (β_i); (d) fluorescence lifetimes (τ_i). All decay transients were measured from 400 to 650 nm with 5 nm increments. The inset in (b) shows the normalized spectra.

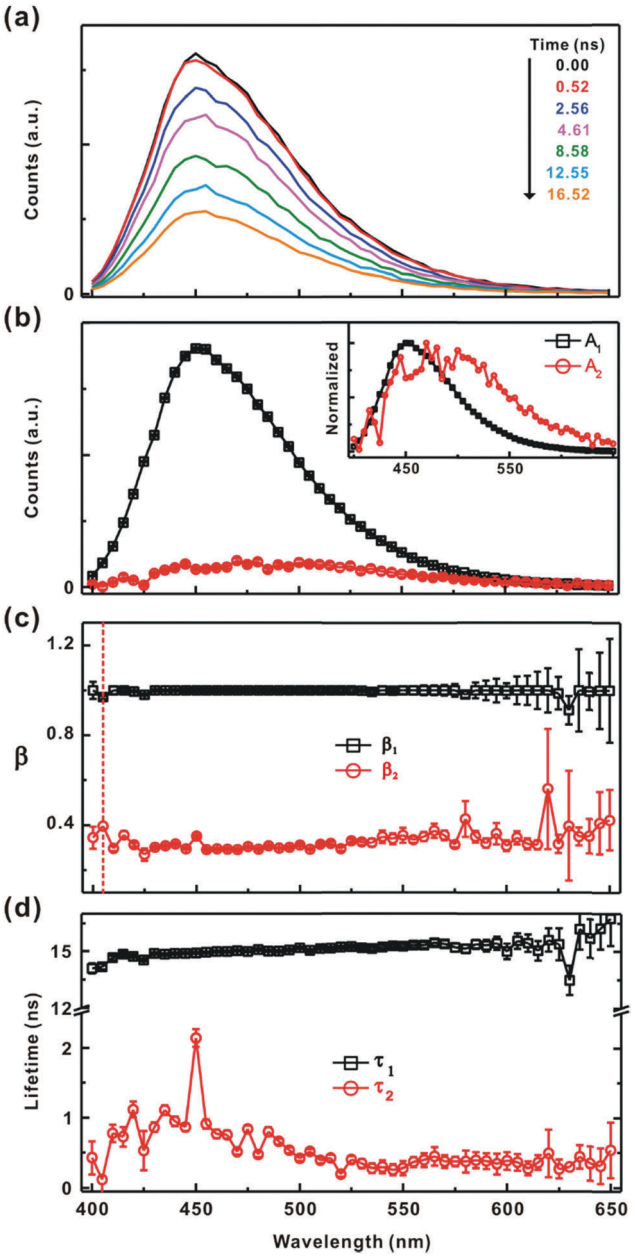

Fig. 6 (a) Time-resolved emission spectra (TRES) of BN-CD with excitation wavelength at 375 nm. Fitting parameters from the stretched-exponential functions are as follows: (b) amplitudes (A_i) of the fluorescence lifetimes; (c) distribution factors (β_i); (d) fluorescence lifetimes (τ_i). All decay transients were measured from 400 to 650 nm with 5 nm increments. The inset in (b) shows the normalized spectra. The vertical dashed line in (c) indicates the error range.

the TRES of N-CD was revisited with $\beta = 1$, as shown in Fig. S6 (ESI†). τ_1 was toward to be uniform ($\tau_1 \sim 15$ ns) across the probed wavelengths, which is self-consistent to the above argument.

When the surface states are selectively excited at 450 nm (for PL profiles, see Fig. S5, ESI†), the TRES peaks (Fig. 7) and related fitting parameters (Table 1) are clearly distinct. Both lifetime distribution factors are significantly smaller than 1 for N-CD ($\beta_1 = 0.8$ and $0.3 \leq \beta_2 \leq 0.6$), and the corresponding lifetimes were $\tau_1 = \sim 5$ ns and $\tau_2 = \sim 200$ ps, respectively. The two components show a PL peak at around 530 nm, which can be assigned to the electronic transition of low-energy surface states related to N-defects. These results confirm that the obtained PL lifetimes of N-CD are more disordered than those of BN-CD owing to the chromophores on the surface of the N-CD. The larger β values represent the distribution of relaxation channels on each chromophore. Different surface functional groups such as C═O and C═N can introduce new energy levels for electronic transitions and cause tuneable emission.[40]

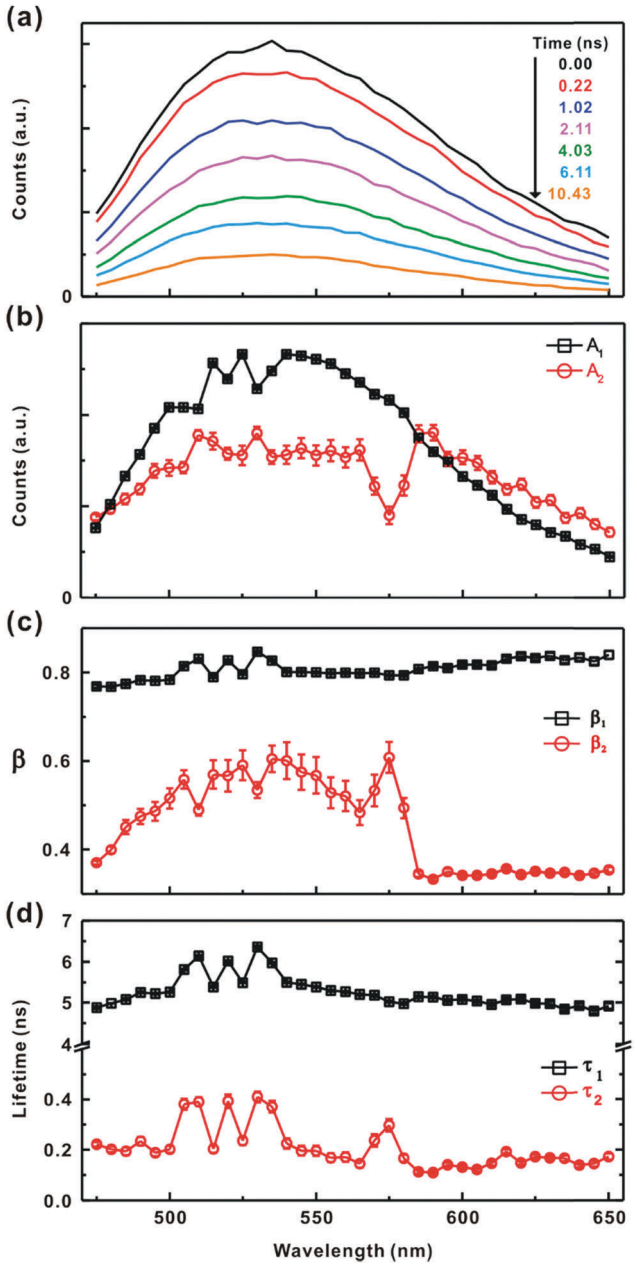

Fig. 7 (a) Time-resolved emission spectra (TRES) of N-CD with excitation wavelength at 450 nm. The fitting parameters from the stretched-exponential functions are as follows: (b) amplitudes (A_i) of the fluorescence lifetimes; (c) distribution factors (β_i); (d) fluorescence lifetimes (τ_i). All decay transients were measured from 400 to 650 nm with 5 nm increments. The inset shows the normalized spectra.

Moreover, the size of the π-conjugated sp^2-domains, which arise from the edge functional groups, may also be distributed. Such distributions seem to induce spectral heterogeneity and non-exponential PL decay patterns. Herein, by analytically comparing the PL decay profiles for the two CDs, which exhibit different λ_{ex} dependence, the variety of surface chromophores is shown to create a series of energy levels for electronic transitions. Khan *et al.* studied the relative population of emitting states, which are responsible for the inhomogeneous broadening of the TRES peaks,[26] and revealed the contribution of relaxed substates for energy redistribution and relaxation among the emitting states on nanosecond timescales, in agreement with our observations herein.

Our summarized PL mechanism for both CDs is shown in Scheme 2. The carbon core domain (grey) is excited at ~250 nm, and the corresponding emission at ~330 nm is very weak (inset in Fig. 1). Taking the relative intensity of the bands at ~330 nm with respect to the bands at ~450 nm, the corresponding lifetimes were estimated to be shorter than 20 ps. These bands originate from the sp^2-core states, which are short-lived owing to the facile energy transfer to the molecular state or to surface states. The ultrashort lifetimes could not be directly measured in this study because of the experimental limitations. The maximum of emission from the molecular state is found at ~450 nm, followed by absorption at ~350 nm. The PL lifetime is estimated to be ~15 ns at ~450 nm for both CDs, and the lifetime is well defined (β = 1.0). The surface states are excited for λ_{ex} > 410 nm, and their PL behaviour is dependent on the chromophoric states.[17] An absorption tail was mainly observed for N-CD beyond ~410 nm. The excitation spectra show multiple band features at ~420 nm, ~450 nm, and ~520 nm (Fig. 2b). Moreover, N-CD has various PL lifetimes (~500 ps–3 ns) originating from the abundant surface states, which are attributed to the versatile distribution of the different surface chromophores responsible for the λ_{ex}-dependent PL.[44,45] On the other hand, the PL lifetimes of the surface states of BN-CD were around 500 ps, but the distribution of the lifetime component at each emission wavelength was wider. This distribution of relatively constant PL lifetimes indicates that the kinds of surface states are less developed but those states experience heterogeneity in local environments. Based on the chemical composition of the CDs (obtained by XPS),[14] N-CDs have dominant carboxylic acid and

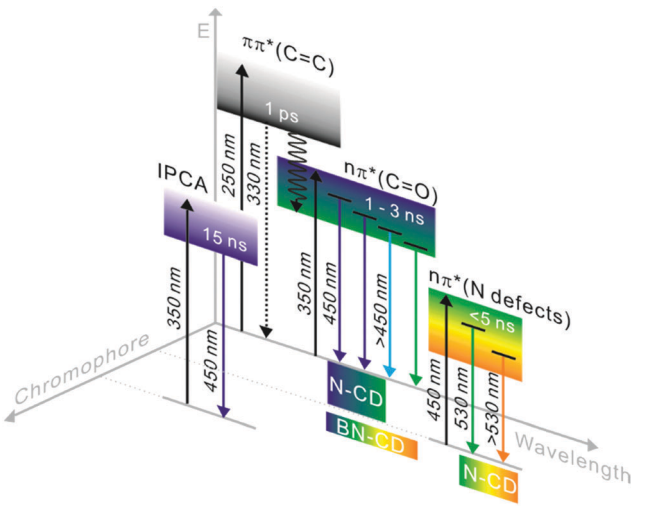

Scheme 2 Energy-level diagram and proposed PL emission mechanisms for N-CD and BN-CD. Multiple emissive states corresponding to the sp^2-carbon-core (C═C), molecular state (from IPCA), and chromophoric surface domains such as nπ* (C═O and N-defects) exist at given wavelengths. Decay (<5 ns) from the lower-lying N-defects states was exclusively observed for N-CD.

pyrrolic-N functional groups, while BN-CDs possess less functional groups with graphitic-N. The carboxylic acid and pyrrolic-N functional groups form multifunctional chemical chromophores, which lead to the λ_{ex}-dependent PL behaviour in N-CDs.

4. Conclusions

We investigated the PL properties of two different CDs by comparing both the steady-state absorption and emission spectra and the time-resolved PL spectra. An excitation-dependent PL behaviour was observed mainly for N-CD, which is due to the different N configurations of significant population. To quantitatively analyse the PL behaviour, the decay profiles of both CDs were fitted by stretched-exponential functions to disentangle the underlying electronic states. This method conclusively supports that the PL of CDs is governed by two representative emissive states: a main molecular state and a sum of multiple electronic states related to the surface functional groups. For both CDs, the molecular state contributes to the strong blue emission with a dominant PL lifetime of $\sim$15 ns, in agreement with previously reported IPCA results. On the other hand, multiple electronic states are responsible for the contrasting excitation dependence in BN-CD and N-CD. These states arise from the diverse surface chromophores, as revealed by the lifetime variation and distributions. We believe that this study may help understand the origin of and quantify the differences in the complex PL behaviour of CDs to design outperforming CDs for future applications.

Conflicts of interest

There are no conflicts to declare.

Acknowledgements

This work was supported by the National Research Foundation of Korea (NRF) funded by the Ministry of Science, ICT and Future Planning (2017R1A2B4010271, 2017R1A6A3A11028305, and 2017M3A7B4052802).

Notes and references

1 S. N. Baker and G. A. Baker, *Angew. Chem., Int. Ed.*, 2010, **49**, 6726–6744.
2 S. Y. Lim, W. Shen and Z. Gao, *Chem. Soc. Rev.*, 2015, **44**, 362–381.
3 H. Li, X. He, Z. Kang, H. Huang, Y. Liu, J. Liu, S. Lian, C. H. Tsang, X. Yang and S. T. Lee, *Angew. Chem., Int. Ed.*, 2010, **49**, 4430–4434.
4 C. Ding, A. Zhu and Y. Tian, *Acc. Chem. Res.*, 2014, **47**, 20–30.
5 C. F. Wang, X. Wu, X. P. Li, W. T. Wang, L. Z. Wang, M. Gu and Q. Li, *J. Mater. Chem.*, 2012, **22**, 15522–15525.
6 Q. L. Wang, X. X. Huang, Y. J. Long, X. L. Wang, H. J. Zhang, R. Zhu, L. P. Liang, P. Teng and H. Z. Zheng, *Carbon*, 2013, **59**, 192–199.
7 V. Georgakilas, J. A. Perman, J. Tucek and R. Zboril, *Chem. Rev.*, 2015, **115**, 4744–4822.
8 L. Zheng, Y. Chi, Y. Dong, J. Lin and B. Wang, *J. Am. Chem. Soc.*, 2009, **131**, 4564–4565.
9 S. L. Hu, K. Y. Niu, J. Sun, J. Yang, N. Q. Zhao and X. W. Du, *J. Mater. Chem.*, 2009, **19**, 484–488.
10 X. Xu, R. Ray, Y. Gu, H. J. Ploehn, L. Gearheart, K. Raker and W. A. Scrivens, *J. Am. Chem. Soc.*, 2004, **126**, 12736–12737.
11 Z. C. Yang, M. Wang, A. M. Yong, S. Y. Wong, X. H. Zhang, H. Tan, A. Y. Chang, X. Li and J. Wang, *Chem. Commun.*, 2011, **47**, 11615–11617.
12 S. Sahu, B. Behera, T. K. Maiti and S. Mohapatra, *Chem. Commun.*, 2012, **48**, 8835–8837.
13 X. H. Wang, K. G. Qu, B. L. Xu, J. S. Ren and X. G. Qu, *J. Mater. Chem.*, 2011, **21**, 2445–2450.
14 Y. Choi, B. Kang, J. Lee, S. Kim, G. T. Kim, H. Kang, B. R. Lee, H. Kim, S. H. Shim, G. Lee, O. H. Kwon and B. S. Kim, *Chem. Mater.*, 2016, **28**, 6840–6847.
15 Y. Q. Zhang, D. K. Ma, Y. Zhuang, X. Zhang, W. Chen, L. L. Hong, Q. X. Yan, K. Yu and S. M. Huang, *J. Mater. Chem.*, 2012, **22**, 16714–16718.
16 Y. Dong, H. Pang, H. B. Yang, C. Guo, J. Shao, Y. Chi, C. M. Li and T. Yu, *Angew. Chem., Int. Ed.*, 2013, **52**, 7800–7804.
17 X. M. Li, S. L. Zhang, S. A. Kulinich, Y. L. Liu and H. B. Zeng, *Sci. Rep.*, 2014, **4**, 4976.
18 D. Qu, M. Zheng, L. Zhang, H. Zhao, Z. Xie, X. Jing, R. E. Haddad, H. Fan and Z. Sun, *Sci. Rep.*, 2014, **4**, 5294.
19 M. Fu, F. Ehrat, Y. Wang, K. Z. Milowska, C. Reckmeier, A. L. Rogach, J. K. Stolarczyk, A. S. Urban and J. Feldmann, *Nano Lett.*, 2015, **15**, 6030–6035.
20 N. Dhenadhayalan, K. C. Lin, R. Suresh and P. Ramamurthy, *J. Phys. Chem. C*, 2016, **120**, 1252–1261.
21 L. Wang, S. J. Zhu, H. Y. Wang, S. N. Qu, Y. L. Zhang, J. H. Zhang, Q. D. Chen, H. L. Xu, W. Han, B. Yang and H. B. Sun, *ACS Nano*, 2014, **8**, 2541–2547.
22 Y. L. Hao, Z. X. Gan, X. B. Zhu, T. H. Li, X. L. Wu and P. K. Chu, *J. Phys. Chem. C*, 2015, **119**, 2956–2962.
23 C. Zheng, X. Q. An and J. Gong, *RSC Adv.*, 2015, **5**, 32319–32322.
24 Y. Choi, S. Kim, Y. Choi, J. Song, T. H. Kwon, O. H. Kwon and B. S. Kim, *Adv. Mater.*, 2017, **29**, 1701075.
25 S. J. Zhu, Y. B. Song, X. H. Zhao, J. R. Shao, J. H. Zhang and B. Yang, *Nano Res.*, 2015, **8**, 355–381.
26 S. Khan, A. Gupta, N. C. Verma and C. K. Nandi, *Nano Lett.*, 2015, **15**, 8300–8305.
27 A. Bhattacharya, S. Chatterjee, R. Prajapati and T. K. Mukherjee, *Phys. Chem. Chem. Phys.*, 2015, **17**, 12833–12840.
28 H. Zheng, Q. Wang, Y. Long, H. Zhang, X. Huang and R. Zhu, *Chem. Commun.*, 2011, **47**, 10650–10652.
29 H. Ding, S. B. Yu, J. S. Wei and H. M. Xiong, *ACS Nano*, 2016, **10**, 484–491.
30 S. Zhu, Q. Meng, L. Wang, J. Zhang, Y. Song, H. Jin, K. Zhang, H. Sun, H. Wang and B. Yang, *Angew. Chem., Int. Ed.*, 2013, **52**, 3953–3957.
31 Y. B. Song, S. J. Zhu, S. T. Zhang, Y. Fu, L. Wang, X. H. Zhao and B. Yang, *J. Mater. Chem. C*, 2015, **3**, 5976–5984.

32 L. Bao, Z. L. Zhang, Z. Q. Tian, L. Zhang, C. Liu, Y. Lin, B. Qi and D. W. Pang, *Adv. Mater.*, 2011, **23**, 5801–5806.
33 S. K. Das, Y. Liu, S. Yeom, D. Y. Kim and C. I. Richards, *Nano Lett.*, 2014, **14**, 620–625.
34 H. Wang, P. Sun, S. Cong, J. Wu, L. Gao, Y. Wang, X. Dai, Q. Yi and G. Zou, *Nanoscale Res. Lett.*, 2016, **11**, 27.
35 O. Kozák, M. Sudolská, G. Pramanik, P. Cígler, M. Otyepka and R. Zbořil, *Chem. Mater.*, 2016, **28**, 4085–4128.
36 A. Sharma, T. Gadly, A. Gupta, A. Ballal, S. K. Ghosh and M. Kumbhakar, *J. Phys. Chem. Lett.*, 2016, **7**, 3695–3702.
37 S. Zhu, Y. Song, X. Zhao, J. Shao, J. Zhang and B. Yang, *Nano Res.*, 2015, **8**, 355–381.
38 M. N. Berberan-Santos, E. N. Bodunov and B. Valeur, *Chem. Phys.*, 2005, **317**, 57–62.
39 P. Yu, X. M. Wen, Y. R. Toh and J. Tang, *J. Phys. Chem. C*, 2012, **116**, 25552–25557.
40 H. Nie, M. J. Li, Q. S. Li, S. J. Liang, Y. Y. Tan, L. Sheng, W. Shi and S. X. A. Zhang, *Chem. Mater.*, 2014, **26**, 3104–3112.
41 M. Roding, S. J. Bradley, M. Nyden and T. Nann, *J. Phys. Chem. C*, 2014, **118**, 30282–30290.
42 A. S. R. Koti, M. M. G. Krishna and N. Periasamy, *J. Phys. Chem. A*, 2001, **105**, 1767–1771.
43 J. Schneider, C. J. Reckmeier, Y. Xiong, M. von Seckendorff, A. S. Susha, P. Kasak and A. L. Rogach, *J. Phys. Chem. C*, 2017, **121**, 2014–2022.
44 Y. P. Sun, B. Zhou, Y. Lin, W. Wang, K. A. Fernando, P. Pathak, M. J. Meziani, B. A. Harruff, X. Wang, H. Wang, P. G. Luo, H. Yang, M. E. Kose, B. Chen, L. M. Veca and S. Y. Xie, *J. Am. Chem. Soc.*, 2006, **128**, 7756–7757.
45 A. P. Demchenko and M. O. Dekaliuk, *Nanoscale*, 2016, **8**, 14057–14069.